Response to Reviewer

1. I cannot agree the conclusions that upward flux of nitrate controls phytoplankton production and patchy distributions. At least, the authors should discuss why Chl a amount remained low while the nutrients were supplied richly at station C6 if the data removed. Additionally, the Chl a amount at C11 was outlier in the relationship. The relationship between Chl a amount and the nitrate upward flux except C6, C9 and C11 showed the significant positive relationship. This relationship indicate that nutrient upward flux basically controls the phytoplankton abundance, however, the patchy Chl a variations (for example at C11 and C6) are not controlled by the upward flux. That is, I consider that the patchiness of Chl a concentration is not largely controlled by the upward flux.

Response: Though nutricline and the depth of chlorophyll maximum were slightly uplifted, station C6 showed relatively lower chlorophyll concentration, which could be caused by along-shelf transport of low-chlorophyll waters over the slope as station C6 was located near the top of the shelf-slope. As has been clearly stated in our previous response, the regression between int-chla and vertical nutrient fluxes is only doable for deep-water stations (C7-C13, A, B) including the offshore pelagic zone and the water intrusion zone. Station C6 should not be included in the regression since it is right on the top of the continental slope subjecting to influence by along-shelf flows. Our regression does not exclude station C11. Integrated chlorophyll and vertical nutrient flux showed a significant correlationship without C9. Therefore phytoplankton patchiness in the offshore NSCS was largely (*but not solely*) controlled by upward flux.

2. The connectivity of the between the line observations (C1-C12) and the stations A, B was unclear. In particular, the area near "station B was well documented for its high turbulent mixing" (L358-360), and so the station B is not the representative station of nSCS. I consider that the observation values such as the phytoplankton growth and the grazing rates in the nSCS cannot be discussed based on the station B data as I pointed out in previous reviews.

Response: The reviewer's argument on this point is nonsense. It is not fair to say that station B is not a representative station of NSCS because of its high turbulent mixing. There are many locations of the NSCS showing high vertical diffusivity. Spatial heterogeneity of turbulent mixing in the NSCS has been well documented as a result of the complex physical dynamics in the NSCS (Tian et al., JPO, 2009; Liu and Losovatsky, 2012).

3. The abstract is the only description of the results and is not organized. I think what new or innovative is necessary to publish in Biogeosciences.

Response: What we have summarized in the abstract is the new findings from results, but not the sorely description of results as claimed by the reviewer. Anyway, we have reorganized the abstract to emphasize more on the major finding and

conclusive remarks from the paper.

Specific Comments
L126: Not only the company, but also the product name is necessary.

Response: done

L136: Bran+Luebbe

Response: done

L192: I understood the calculation.   However, the calculated nutrient gradient is not at the depth of Zi.   It was at the depth of (Zi + Zi+1)/2.

Response: It is impossible to calculate gradient at depth of $(Z_i + Z_{i+1})/2$ since there is not data at this depth. On the other hand, one can argue that the gradient calculated from Zi to $(Z_i + Z_{i+1})/2$ would be the same as the gradient calculated from Z_i to Z_{i+1} by linear interpolation.

L471: "n ="

Response: done

Phytoplankton dynamics driven by vertical nutrient fluxes during the spring inter-monsoon period in the northeastern South China Sea

Qian P. Li[*], Yuan Dong, Yanjun Wang

South China Sea Institute of Oceanology, Chinese Academy of Sciences, Guangzhou, China

Correspondence to: qianli@scsio.ac.cn

Abstract

A field survey from the coastal ocean zones to the offshore pelagic zones of the northeastern South China Sea (nSCS) was conducted during the inter-monsoon period of May 2014 when the region was characterized by prevailing low-nutrient conditions. Comprehensive field measurements were made for not only hydrographic and biogeochemical properties but also phytoplankton growth and microzooplankton grazing rates. We also performed estimations of the vertical turbulent diffusivity and diffusive nutrient fluxes using a Thorpe-scale method and the upwelling nutrient fluxes by Ekman pumping using satellite-derived wind stress curl. Our results revealed a positive correlationship between the integrated phytoplankton chlorophyll-a and vertical nutrient fluxes in the offshore region of the nSCS during the study period. We found a generally increasing role of turbulent diffusion but decreasing role of curl-driven upwelling on vertical transport of nutrients from the coastal ocean zones to the offshore pelagic zones in the nSCS. Elevated nutrient fluxes near Dongsha Islands supported high new production leading to net growth of phytoplankton community, whereas the low nutrient fluxes near southwest Taiwan had resulted in a negative net community growth leading to decline of a surface phytoplankton bloom. Overall, phytoplankton dynamics in the large part of the nSCS are largely driven by vertical nutrient fluxes including turbulent diffusion and curl-driven upwelling during the spring inter-monsoon period.

1. **Introduction**

Nutrient fluxes from below the euphotic zone are essential for phytoplankton primary production in the surface ocean (Eppley and Peterson, 1979), while the mechanisms regulating those fluxes are still inadequately understood in the northeastern South China Sea (nSCS), particularly during the spring intermonsoon period. Wind-driven coastal upwelling, river discharge, and inter-shelf nutrient transport were important mechanisms supplying nutrients to the euphotic zone of the nSCS (Liu et al., 2002; Gan et al., 2010; Han et al., 2013), while their contributions to primary production were mostly limited to coastal regions as these nutrients would be mostly utilized in the coastal waters before reaching the large area of the nSCS. Kuroshio intrusion would dilute the nSCS waters with the low nutrient North Pacific waters (Farris and Wimbush. 1996), which appeared to be much weaker during April-September (Centurioni et al., 2004). Contribution of nitrogen fixation to new production of the nSCS was generally negligible compared to the nitrate-based new production (Chen et al., 2005; Bombar et al., 2010). Atmospheric deposition of anthropogenic nitrogen could support up to ~20% of the annual new production in the nSCS exceeding those from riverine inputs (Kim et al., 2014). But its contribution would be much less during the spring inter-monsoon season as the reduced rate of atmospheric deposition (Lin et al., 2009).

Diapycnal mixing by turbulent dissipation was recently found to be important for the supply of new nitrogen in the nSCS, where the vertical turbulent diffusivities were an order of magnitude higher than the adjacent West Pacific Ocean (Tian et al., 2009; Liu and Lozovatsky 2012; Yang et al., 2014). It was also suggested that phytoplankton blooms off the west coast of the nSCS could be induced by wind stress curl-driven upwelling during the spring inter-monsoon season (Wang and Tang 2014), which would cause a local uplift of isopycnals leading to nutrient injection into the euphotic zone with subsequent changes of community structure and productivity (Rykaczewski and Checkley 2008; Li et al., 2015). By modifying the surface wind stress and wind stress curl via air-sea coupling, the eddy-induced Ekman pumping (Gaube et al., 2013) was important for phytoplankton production in the nSCS during the inter-monsoon transition period (Lin et al., 2010). As both intermittent turbulent diffusion and wind-driven Ekman pumping affect the vertical transport of nutrients on temporal scales similar to the generation time

of phytoplankton, they will have large influences on plankton dynamics of the upper ocean (Cullen et al., 2002). It is therefore important to investigate the roles of these two mechanisms in driving the variability of phytoplankton biomass and primary production in the large area of the nSCS.

Spatial distribution of phytoplankton at sea is a result of complex interactions between physical and biological processes (Davis et al., 1991; Abraham 1998). In addition to the vertical nutrient fluxes, phytoplankton biomass and productivity of the nSCS are influenced by growth-grazing dynamics (Chen 2005; Huang et al., 2011; Zhou et al., 2011; Chen et al., 2013). Shifts in the dominance of phytoplankton species in the western South China Sea were believed to be driven by a close coupling of the mortality rates of different phytoplankton groups via common grazers such as nanoflagellates (Chen et al., 2009). There was on average ~61% of phytoplankton growth lost to microzooplankton grazing in coastal upwelling regions of the nSCS in response to increased nutrient fluxes, whereas growth and grazing mortality rates were mostly balanced on the shelf and shelf break areas without upwelling events (Huang et al., 2011). It was also suggested that the balance of phytoplankton growth and microzooplankton grazing in the pelagic nSCS could be perturbed by physical disturbances such as eddies, fronts, and typhoons, leading to large deviations of planktonic ecosystem from the steady state (Zhou et al., 2011; Chen et al., 2013).

Here, we present results of a field survey from the coastal ocean zones to the offshore pelagic zones in the nSCS conducted during the spring inter-monsoon transition of May 2014, when the region was characterized by prevailing low nutrient conditions as a result of weak and variable winds (Lin et al., 2010). Comprehensive measurements were made for hydrographic and biogeochemical properties, as well as biological rates including phytoplankton growth and grazing rates and net nutrient consumption rates. We also performed estimations of the vertical turbulent diffusivity and diffusive nutrient fluxes using a Thorpe-scale method (Gargett and Garner 2008; Li et al., 2012) and the upwelling nutrient fluxes by Ekman pumping using satellite-derived wind stress curl (Gill 1982; Risien and Chelton 2008). In synthesizing these field data, the focus of this paper are to (1) investigate the spatial patterns of vertical nutrient fluxes in the nSCS, (2) determine the relative roles of turbulent diffusion and Ekman pumping to vertical transport of

98   nutrients in the upper ocean, and (3) understand the linkage between vertical nutrient

99   fluxes and phytoplankton dynamics in the nSCS during the spring inter-monsoon period.

100

101   **2. Materials and methods**

102   2.1.Site description, field sampling, and measurements

103   There are typically high nutrients in the coastal regions of the nSCS due to river

104   discharge, inter-shelf transport, and upwelling and mixing (Gan et al., 2010), in contrast

105   to the oligotrophic low-latitude offshore regions with strong stratification. The nSCS is

106   also strongly influenced by Kuroshio intrusion through the Luzon Strait (Farris and

107   Wimbush 1996). The intruded Kuroshio waters with higher temperature and salinity but

108   lower nutrients are often transported westward via eddies and Ekman advection

109   (Centurioni et al., 2004) influencing the large area of the nSCS on seasonal time-scales.

110   A field survey of the nSCS (Fig. 1) was conducted during May 2014 aboard the *R/V*

111   *Shiyan III* of the South China Sea Institute of Oceanology. From May 14th to May 16th,

112   2014, a transect from the coastal waters near Shantou to the offshore waters near the

113   Luzon Strait was comprehensively sampled to investigate the spatial patterns of

114   hydrographic and biogeochemical properties of the nSCS. Station S_1 (22°N, 119.5°E) was

115   chosen as a reference time-series station with continuous CTD sampling of 13 casts

116   within 24 hours (start: 10:00 am, May 18th, 2014). Stations A (21.9°N, 120°E with a

117   bottom depth of 1547 m) near the southwest of Taiwan and station B (20.5°N, 117°E with

118   a bottom depth of 607 m) in the southeast of Dongsha Islands were selected for dilution

119   experiments to quantify phytoplankton growth and microzooplankton grazing rates.

120   Discrete seawater samples at depths of 0 m, 25 m, 50 m, 75 m, 100 m, 200 m, 300 m,

121   500 m, and 700 m were collected using a SeaBird SBE 9/11 CTD rosette water sampler

122   system, providing high resolution hydrographic measurements of the upper water column

123   with internal pressure, conductivity, and temperature sensors. We define euphotic zone as

124   the layer above 1% of surface Photosynthetically Active Radiation (PAR), measured by a

125   PAR sensor (QSP200L, Biospherical Instrument, Inc.). After inline filtrations from the

126   PVC Niskin bottles through 0.8 μm Nuclepore filters, seawater samples for nutrients

127   were frozen immediately and stored in a refrigerator until final analyses after the cruise.

128   For chlorophyll-*a* sampling, 500 ml of seawater was gently filtered (<50 mmHg) through

129   a GF/F (Whatman) filter, which was wrapped in a piece of aluminum foil and kept at

130   -20°C on board. Upon return to the lab, chlorophyll-*a* samples were sonicated for 20 min

131   and extracted in 5 ml 90% acetone at 4°C in the dark for 24 hours. These samples were

132   centrifuged at 4000 rpm for 10 min before final determinations by standard fluorescence

133   methods (Parsons et al., 1984) using a Turner Designs Model 10 Fluorometer.

134   Concentrations of nitrate plus nitrite, phosphate and silicate were determined by a Seal

135   AA3 auto analyzer (Bran-Luebbe, GmbH). The low concentrations of nitrate plus nitrite

136   and phosphate within the euphotic zone were also determined by the long-cell method (Li

137   et al., 2008; Li and Hansell 2008) by incorporating a 50 cm liquid waveguide cell to AA3

138   with detection limits of ~0.02 μM and ~0.01 μM, respectively.

139

140   2.2. Remote sensing observations

141   High-resolution satellite data, including sea surface temperature (SST), sea surface

142   chlorophyll (SSChl), surface geostrophic velocities, as well as surface wind stresses and

143   Ekman velocities, were used to assess the spatial change of these surface properties in the

144   nSCS during the study period. Monthly averaged sea surface chlorophyll-*a* (0.04°×0.04°)

145   was acquired from the NASA's Moderate Resolution Imaging Spectroradiometer data

146   observed by the Aqua Satellite (MODIS-Aqua). Five-day-mean surface velocity fields

147   (0.3°×0.3°) were derived from multi-satellite altimeter (TOPEX, JASON-1, ERS-2,

148   ENVISAT and GFO) and scatterometer data distributed by the NOAA's Ocean Surface

149   Current Analysis -Realtime (OSCAR) program, which had been largely validated by a

150   variety of field measurements including global drifts, moorings, and shipboard ADCP.

151   Daily sea surface temperature (0.1°×0.1°) was acquired from the NOAA's Geostationary

152   Operational Environmental Satellite –Polar Operational Environmental Satellite program

153   (GOES-POES). Daily Ekman upwelling velocities and surface wind stresses with a

154   resolution of 0.25°×0.25° were derived from the Advanced Scatterometer data by the

155   European Meteorological and Operational satellite program (METOP-ASCAT). The

156   Ekman pumping velocity (w_e, negative for downwelling) at the depth of Ekman layer is

157   calculated as (Gill, 1982)

158

$$w_e = \frac{1}{\rho_w}\left(\nabla \times \frac{\tau}{f}\right)$$

159   (1)

160   where ρ_w is the density of seawater, which is assumed constant at 1024 kg m^{-3}; f is the

161   Coriolis parameter; τ is the vector of wind stress.

162

163   2.3 Thorpe-scale analyses and vertical diffusivity

164   We applied a Thorpe-scale based approach (Thorpe 1977; Galbraith and Kelley 1996;

165   Gargett and Garner 2008; Li et al., 2012) to estimate fine structure and turbulent

166   diffusivity for each station using CTD downcast data. The method combines several

167   criteria to determine the real overturns from a density profile (Li et al., 2012), including

168   the test of minimum thickness, the run-length and water mass tests (Galbraith and Kelley

169   1996), as well as the tests of minimal overturn ratio and maximal T/S tightness (Gargett

170   and Garner 2008). These criteria ensure that the maximal density difference within an

171   overturn is greater than twice the measurement noise (0.001 kg m^{-3}). The length scale of

172   an overturn is larger than twice the vertical resolution (Nyquist theorem) and larger than a

173   minimum thickness (Galbraith and Kelley 1996). The percentage of positive/negative

174   displacements within an overturn (the overturn ratio) is larger than 0.2 and the deviations

175   on a T/S diagram are less than 0.003 (Gargett and Garner 2008). The vertical resolution

176   of CTD sampling during the cruise was ~10 cm with a fall rate of ~2.4 m s^{-1}. Therefore,

177   only overturns larger than 0.5 m are included, to obtain five data point resolution. We

178   discard data in the upper 10 m, as the Thorpe approach is not strictly valid there. Once an

179   overturn is identified, the Thorpe scale (L_T) is calculated from the root mean square of the

180   vertical displacement (d_z) as $L_T = (\Sigma d_z^2)^{0.5}$.

181   Turbulent kinetic energy dissipation rate (ε) is calculated from L_T and N by

182    $$\varepsilon = 0.64 \cdot L_T^2 \cdot N^3$$

183   (2)

184   where N is the buoyancy frequency given by $N^2 = -g\rho_0^{-1}(\partial\rho/\partial z)$ with g the gravitational

185   acceleration, ρ_0 the mean density, and $\partial\rho/\partial z$ the density gradient across each overturn

186   (Galbraith and Kelley 1996). According to Osborn (1980), the vertical diffusivity (K_z) can

187   be estimated from ε and N by

188    $$K_z = 0.2 \cdot \varepsilon \cdot N^{-2}$$

189   (3)

190   The diffusive nutrient fluxes at the depth of interest can be estimated by multiplying the

191   diffusivity (K_z) by the local nutrient gradient ($\partial C/\partial z$). Nutrient gradient, at the depth of Z_i

192   with the concentration of C_i, is approximately estimated by $(C_{i+1}-C_i)/(Z_{i+1}-Z_i)$, with C_{i+1}

193   the concentrations at Z_{i+1} immediately next to Z_i.

194

195   2.4 Setup of dilution experiments

196   Phytoplankton growth and microzooplankton grazing in the surface waters of stations

197   A and B near the edge of continental shelf were assessed on board using dilution

198   technique (Landry and Hassett 1982; Landry et al., 1998; Li et al., 2011) on May 13th and

199   May 17th, 2014. All the bottles, tubing and carboys were soaked in 10% (v/v)

200   hydrochloric acid solution for over 24 hours and they were rinsed several times with

201   deionized water and seawater before each experiment. Surface seawater, collected by an

202   acid-washed polyethylene bucket, was screened through a 200-µm mesh before being

203   transferred into polycarbonate carboys as raw seawater. A dilution series was prepared

204   with 0%, 25%, 50%, 75%, and 100% unfiltered seawater in duplicated polycarbonate

205   bottles (0% unfiltered seawater sample was not performed at station B). Measured

206   amounts of particle-free seawater, obtained by filtering the raw seawater with 0.45 µm

207   filters, were added to 2.4-liter polycarbonate bottles. These samples were then enriched

208   with additional nutrients to promote constant growth of phytoplankton. Finally, each

209   bottle was gently filled with unfiltered seawater to its capacity. There was also one bottle

210   filled with 100% unfiltered raw seawater without nutrient enrichment to serve as the

211   control for our experiment. All the bottles were tightly capped and incubated for 24 hours

212   in a deck incubator, which was covered with a neutral density screen to mimic the natural

213   sunlight and filled with flowing seawater from the sea surface to control the temperature.

214   Duplicate 300 ml samples were taken from each bottle before and after the dilution

215   experiments for chlorophyll-*a* measurements.

216   Specific rates of nutrient-saturated phytoplankton growth (μ_n, d^{-1}) and

217   microzooplankton grazing (g, d^{-1}) are estimated by least-square regression between the

218   net growth rates (η, d^{-1}) and the dilution factors (D) as

$$\eta = \frac{1}{t} \ln\left(\frac{P_t}{P_0}\right) = \mu_n - D \cdot g$$

219

220
$$(4)$$

221 where P_0 and P_t are the initial and final concentrations of chlorophyll-a, respectively and

222 t is the duration of the incubation. The natural phytoplankton growth rate (μ), which is

223 often subjected to nutrient limitation (Landry et al., 1998), is finally estimated from the

224 net growth rate of raw seawater without nutrient enrichment (η_{raw}) by $\mu = \eta_{raw} + g$.

225   To examine the response of the phytoplankton community to nutrient enrichment, two

226 bottles of raw seawater with nutrient additions were incubated for 4 days, with

227 chlorophyll-a and nutrient samples taken at the very beginning and each day afterwards.

228 Nutrient data within the exponential growth phase is used to estimate the specific net

229 nutrient consumption rate (m) of the incubated community by linear regression of $ln(C)$

230 and t assuming

231
$$\frac{dC}{dt} = -m \cdot C$$

232
$$(5)$$

233 where C is the concentration of dissolved nutrients in the sample.

234

235 **3. Results**

236 3.1 Hydrographic dynamics of the nSCS

237   During the survey of May 2014, waters of the nSCS can be grouped into three regions

238 (Fig. 1): the coastal ocean zone (stations C_{1-6}), the offshore pelagic zone (stations C_{7-10}),

239 and the water-intrusion zone near the Luzon Strait (stations C_{11-13}). These three different

240 zones were influenced by a diverse set of physical processes. The coastal ocean zone,

241 which can be further separated into two subregions including the nearshore area (stations

242 C_{1-2}) and the continental shelf (stations C_{3-6}), was strongly affected by wind-driven

243 upwelling processes including Ekman transport and Ekman pumping (Gan et al., 2010).

244 The nearshore area was characterized by low sea surface temperature (Fig. 2a) as a result

245 of upwelling via Ekman transport driven by southwest monsoon along the shore. Ekman

246 pumping induced by wind stress curl showed a significant increase near the edge of the

247 continental shelf far away from the coastline (Fig. 2b). Upward transport of the deeper

248   water with lower temperature but higher salinity along the shelf slope was clearly seen

249   during the transect (Fig. 3a and 3b), which could be a result of direct upwelling or

250   alongshore advection of upwelled waters from upstream. Both the offshore pelagic zone

251   and the water-intrusion zone are far from the coast with bottom depths more than 2000 m

252   (Fig. 1). The offshore pelagic zone was relatively stable with weak surface geostrophic

253   currents, while the water-intrusion zone was strongly influenced by Kuroshio intrusion

254   through the Luzon Strait (Fig. 2a).

255   Sea surface temperature from satellite showed a generally increasing trend from the

256   coastal regions near Shantou to the offshore regions near Luzon Strait due to the

257   decreasing latitude (Fig. 2a). The observed cross-shelf gradient of surface temperature

258   from the discrete bottle measurements is in good agreement with the satellite SST data,

259   with an average of 24.0 ± 0.6 $^{\circ}$C near the coast, 25.2 ± 0.2 $^{\circ}$C on the continental shelf,

260   28.4 ± 0.5 $^{\circ}$C in the offshore pelagic zone, and 29.1 ± 0.5 $^{\circ}$C near the Luzon Strait (Fig.

261   3a). Surface salinity was less variable than temperature from nearshore to offshore with a

262   difference of less than 0.3 during the survey (Fig. 3b). Although there was slightly higher

263   surface salinity on the continental shelf (34.1 ± 0.1), the average salinity concentration at

264   the surface in the coastal ocean zone (33.9 ± 0.2) was generally the same as those of the

265   offshore pelagic zone (33.8 ± 0.1) and the water-intrusion zone (33.9 ± 0.3). Substantially

266   higher subsurface salinities within the euphotic zone between the offshore pelagic zone

267   and the water-intrusion zone (Fig. 3b) could come from the upwelled Pacific waters

268   southwest of Taiwan (Chao et al., 1996).

269   Directions of wind stresses in the nSCS were generally southwest during the study

270   period except two regions where wind stress changed direction (vectors of Fig. 2b): one

271   in the northwest of Dongsha Islands with southerly winds and the other in the Luzon

272   Strait with westerly winds. There were several places of curl-driven upwelling in the

273   offshore deep-water regions, though the entire area was predominantly downwelling.

274   Large curl-driven upwelling ($>0.5 \times 10^{-5}$ m s^{-1}) was only observed near the edge of the

275   continental shelf over abrupt changes of bathymetry. Strong temporal variations of

276   Ekman pumping velocity (Fig. 2d) could be found in the coastal station of C_6 and the

277   offshore station of C_{13}. Though the vertical velocities by Ekman pumping during our

278   sampling duration of May 14th-16th, 2014 are relatively low, they are representative of the

279 entire spring intermonsoon period from May 8th to June 7th, 2014 with substantially low

280 wind intensity (Fig. 2d).

281

282 3.2 Spatial patterns of chlorophyll-*a* and nutrients in the nSCS

283   Sea surface chlorophyll-*a* in the nSCS during May 2014 was very high in the coastal

284 ocean zone – particularly in the near-shore regions – and decreased slightly on the

285 continental shelf (Fig. 2c). In contrast, there was generally low sea surface chlorophyll-*a*

286 in the large areas of the offshore pelagic zone and the water-intrusion zone.

287 Concentrations of the surface chlorophyll-*a* from discrete measurements during our

288 survey (Fig. 3c), varying from 0.04 to 0.92 µg L^{-1}, is in good agreement with the satellite

289 remote sensing data. In particular, surface chlorophyll-*a* along the section shows a

290 general seaward-decreasing trend from the costal regions of 0.72 ± 0.36 µg L^{-1} to the

291 offshore regions of 0.09 ± 0.04 µg L^{-1}, which is consistent with the decrease of surface

292 nitrate concentrations from >1.0 µmol L^{-1} near coast to <1.0 µmol L^{-1} in offshore (Fig.

293 3d). There was a surface chlorophyll patch (~0.3 µg L^{-1}) found at station C_{11} between the

294 offshore pelagic zone and the water-intrusion zone during the transect study (Fig. 3c),

295 which could result from a surface phytoplankton bloom spreading from the southwest

296 coast of Taiwan to the offshore regions of the central nSCS (Fig. 2c).

297   Phytoplankton chlorophyll-*a* was vertically well mixed in the coastal ocean zone,

298 with clear subsurface maxima of chlorophyll-*a* only found in the offshore pelagic zone

299 and the water-intrusion zone (Fig. 3c). The depth of the subsurface chlorophyll maxima

300 followed the $\sigma_{\theta\,=}$ 23.5 isopycnal, which became much shallower when approaching the

301 continental shelf from offshore. The vertical distribution of nutrients along the section

302 generally followed the isopycnal surfaces in the upper water column (Fig. 3d-f), revealing

303 the importance of physical control on upper ocean biogeochemistry. The observed uplifts

304 of isopycnals as well as the depths of chlorophyll maximum and nutricline at stations C_6,

305 C_8, C_9, C_{10}, and C_{12} are consistent with positive upwelling velocities driven by wind

306 stress curl (Fig. 2b). Interestingly, there were substantially higher phosphate and silicate

307 concentrations at depths of ~200 m (across the $\sigma_\theta = 25.5$ isopycnal) for both stations C_9

308 and C_{11} in the offshore regions, which could be due to either a horizontal or vertical

309 injection event prior to our survey. Elevated chlorophyll-*a* at station C_{11} was

310 accompanied by not only the subsurface high nutrients but also the high salinity in the

311 euphotic zone, suggesting possible vertical and horizontal nutrient transports in the upper

312 layer. Curiously, low chlorophyll-*a* was found at station C_9, which showed the highest

313 nutrient concentrations and nutrient gradients. Along the density interval of $\sigma_\theta = 25$ and σ_θ

314 $_= 26$ in the water-intrusion zone there was evidence for isopycnal mixing between the

315 high-nutrient nSCS waters and the adjacent waters of Luzon Strait with lower nutrient but

316 higher temperature/salinity.

317

318 3.3 Vertical diffusivity and diffusive nutrient fluxes

319   Turbulent diffusivity estimated by Thorpe analyses varied substantially from the edge

320 of continental shelf to the west of Luzon Strait during May 2014 (Fig. 4). An overall

321 averaged K_z of 2.5×10^{-4} m^2 s^{-1} for the upper 300 m of the offshore deep-water stations is

322 much higher than the oceanic background diffusivity of 10^{-5} m^2 s^{-1}, but is comparable to

323 the previous basin-scale estimates in the nSCS (Tian et al., 2009; Liu and Lozovatsky

324 2012). There were relatively high mean diffusivities of 3.6×10^{-4} and 3.3×10^{-4} m^2 s^{-1} at

325 stations C_8 and C_{11}, compared to 2.5×10^{-5} m^2 s^{-1} of station C_9. Although the nitrate

326 gradient at the based of euphotic zone in C_9 (0.12 mmol m^{-2}) was about twice of that in

327 C_{11} (0.06 mmol m^{-2}), its diffusive nitrate flux (0.26 mmol m^{-2} d^{-1}) was only about 15% of

328 that in C_{11}. Our data reveals a general decreasing of mean diffusivity from 1.1×10^{-3} m^2 s^{-1}

329 of C_5 on the continental shelf, to 6.3×10^{-4} m^2 s^{-1} of C_6 over the continental slope, and to

330 9.1×10^{-5} m^2 s^{-1} of C_7 in the offshore pelagic zone. Yang et al. (2014) measured turbulent

331 diffusivity along a short section near the edge of the continental shelf southwest of

332 Taiwan using a microstructure profiler during May 2004 – about the same place as our

333 stations C_5 to C_7 (Fig. 1). Their results showed high turbulent mixing over the continental

334 shelf with a mean diffusivity of 1.6×10^{-3} m^2 s^{-1} but a much lower diffusivity of 5.2×10^{-4}

335 m^2 s^{-1} over the slope (Yang et al., 2014), which are well comparable with our estimates

336 using Thorpe analyses.

337   Due to intermittent nature of the turbulence dissipation, the vertical structures of

338 diffusivity observed during our study were quite patchy (Fig. 4). In order to investigate

339 the vertical patterns of turbulent diffusivity, we compared the observations of the two

340 incubation stations (stations A and B) with that of the reference time-series station S_1 (Fig.

15

341 5), which had a better vertical resolution of diffusivity. It is not surprising to find that the

342 diffusivity profile of station A is quite similar to that of station S_1 (Fig. 5), as the two

343 stations are very close to each other (Fig. 1). However, there are substantially higher

344 diffusivities found in station B than in station S_1 (Fig. 5). The average diffusivity at 100 m

345 during our study was about 1.6×10^{-4} m^2 s^{-1} in station A but about 4.4×10^{-4} m^2 s^{-1} in station

346 B. The corresponding diffusive nitrate fluxes at the base of euphotic zone were thus about

347 0.65 mmol m^{-2} d^{-1} in station A and 3.03 mmol m^{-2} d^{-1} in station B, given their nitrate

348 gradients of 0.05 and 0.08 mmol m^{-2} at 100 m, respectively (Table 1). Region of the

349 southeast Dongsha Islands near station B has been well documented for its high turbulent

350 mixing because of internal waves (e.g. Lien et al., 2005; Chow et al., 2008). Enhanced

351 vertical mixing by nonlinear internal waves generated at the shelf edge near Dongsha

352 Islands (Lien et al., 2005) would lead to a higher surface chlorophyll-*a* and net primary

353 production than the adjacent areas with less influence of internal waves during the

354 summertime (Pan et al., 2012). The high diffusivity and diffusive nitrate flux at station B

355 may also be contributed by physical dynamics associated with high internal waves found

356 in this region. The frontal zones at the edge of eddies are often places of increased

357 vertical mixing (Klein and Lapeyre 2009; Li et al., 2012), though the eddy-induced

358 vertical fluxes may vary substantially between cyclonic, anticyclonic and mode-water

359 eddies (McGillicuddy et al., 2007).

360

361 3.4 Rates of phytoplankton growth, microzooplankton grazing, and specific nutrient

362 consumption

363   Hydrographic and biogeochemical conditions of the two incubation stations were

364 quite different, with much higher temperature (Fig. 6) and salinity (data not shown) but

365 lower nutrients and nutrient gradients in station A than in station B (Fig. 6). Station A was

366 at the edge of a surface phytoplankton bloom (Fig. 2c) spreading from the southwest

367 coast of Taiwan to the offshore pelagic regions, while station B was near the central nSCS

368 with very low sea surface chlorophyll-*a* (<0.1 μg L^{-1}). Except for the surface layer,

369 chlorophyll-*a* concentration of station B was generally much higher than that of station A

370 throughout the water column. There was a clear subsurface chlorophyll maximum of ~0.4

371 μg L^{-1} at 50 m for station B (Fig. 6), while double peaks of chlorophyll-*a* were found for

372   station A with a surface maximum of ~0.3 μg L^{-1} and a subsurface maximum of ~0.1 μg

373   L^{-1} at 75 m.

374   Rates of phytoplankton growth and microzooplankton grazing at the surface were

375   substantially different between the two stations. The nutrient-saturated phytoplankton

376   growth rate was 1.24 d^{-1} at station B, which was about three times of that at station A

377   (0.44 d^{-1}). On the other hand, the microzooplankton grazing rate of 0.43 d^{-1} at station A

378   was only slightly lower than the grazing rate of 0.60 d^{-1} at station B (Fig. 7). The natural

379   growth rate of phytoplankton, after correction for the effects of nutrient enrichment as

380   described in section 2.3, was 0.28 d^{-1} at station A, much lower than the rate of 1.18 d^{-1} in

381   station B. The rates measured at station B during May 2014 are comparable with previous

382   estimates of growth rates of 1.03 d^{-1} and grazing rates of 0.62 d^{-1} near Dongsha Islands

383   during July 2009 (Chen et al., 2013). Our results for station A are also in good agreement

384   with those found in the non-upwelling area of the south Taiwan Strait (Huang et al., 2011),

385   which suggested mean rates of 0.4-0.5 d^{-1} and 0.3-0.7 d^{-1} for phytoplankton growth and

386   microzooplankton grazing during July 2004 and 2005.

387   Incubation experiments in station A revealed an exponential growth of phytoplankton

388   chlorophyll-*a* in response to nutrient addition within the first two days, before reaching a

389   stable growth phase on the third day and a decay phase on the fourth day; the

390   chlorophyll-*a* of the control experiment with raw seawater without nutrient additions

391   quickly decreased as nutrients were consumed in the bottles (Fig. 8a). In contrast,

392   phytoplankton of station B showed no response to nutrient enrichment within the first two

393   days of incubation compared to the control experiment (Fig. 8b). Significant increase of

394   incubated chlorophyll-*a* for station B was only found during the last two days of

395   experiment (Fig. 8b). Nutrient utilization during nutrient-enrichment incubations at these

396   two stations were also quite different, with a much slower specific rate of nutrient

397   consumption at station B (0.46 d^{-1}) than at station A (1.03 d^{-1}). These results suggest that

398   there was stronger nutrient limitation of the phytoplankton community at station A than

399   station B during our cruise.

400

401   **4. Discussion**

402   4. 1 Roles of turbulent mixing and curl-driven upwelling on nutrient fluxes of the nSCS

403   during the spring inter-monsoon transition period

404   If the horizontal and atmospheric inputs are ignored, the total nutrient flux into the

405   euphotic zone (J_{total}) is the sum of diffusive flux due to turbulent dissipation ($J_{dif}=K_z\partial C/\partial z$)

406   and the advective flux due to upwelling ($J_{upw}=wC$, negative for downwelling):

407
$$J_{total} = K_z \frac{\partial C}{\partial z} + wC$$

408   (6)

409   To assess the roles of turbulent diffusion and Ekman pumping on vertical transport of

410   nutrients in the nSCS, the diffusive and advective nitrate fluxes at the base of euphotic

411   zone was estimated from the continental shelf to the open sea during May 2014 (see

412   Table 1 for details). Vertical velocity (w) at the based of euphotic zone is assumed equal

413   to the curl-driven upwelling/downwelling velocity (w_e) by Ekman pumping. We have

414   neglected Ekman transport as its effect is restricted only to the near coast (Gan et al.,

415   2010). Variations of w during the transect study is consistent with the isopycnal

416   oscillation along the section (Fig. 3), suggesting the important role of Ekman pumping on

417   physical dynamics of the water column. At the continental slope of station C_6, the vertical

418   nitrate fluxes were largely supported by curl-driven upwelling, with turbulent mixing

419   playing a minor role due to low nitrate gradients. In contrast, the diffusive nitrate flux

420   was over three times of the upwelled nitrate flux at station C_7, immediately adjacent to C_6.

421   Except for station C_{12}, curl-driven downwelling was observed in the deep-water regions

422   during the transect study, leading to downward transport of the low-nutrient surface water

423   to the deeper layer. The upward nitrate fluxes in these stations were thus determined by

424   the intensities of diffusive fluxes working against the downwelling fluxes. There was a

425   negative nitrate flux found at station C_9 where downwelling was stronger than the upward

426   diffusion, resulting in a loss of nitrate from the euphotic zone. Our findings suggest that it

427   is the interplay of turbulent diffusion and curl-driven upwelling/downwelling that

428   controls the vertical fluxes of nutrients into the euphotic zone to support phytoplankton

429   production in the nSCS.

430   For the deep-water stations including the offshore pelagic zone and the water

431   intrusion zone, the integrated chlorophyll-a biomass during the transect study shows a

432   positive correlation with the upward nitrate flux ($\int Chl \cdot dz = 16.75 \times J_{total} + 7.7$, $r^2 = 0.58$,

18

433   p=0.014) when stations C_9 is not included (Table 1), supporting the important role of

434   bottom-up control on phytoplankton production in our study area (Chen 2005). From the

435   slope of 16.75, we could estimate a specific new production by vertical nitrate supply of

436   0.060 molN (gChl)$^{-1}$ d^{-1}, which is slightly lower than 0.063-0.088 molN (gChl)$^{-1}$ d^{-1}

437   reported in the nSCS by Chen (2005). Assuming a vertically constant rate of

438   phytoplankton specific growth, a gram chlorophyll-to-carbon ratio of 0.03 and a molar

439   C/N ratio of 6.625, we estimate a vertically integrated primary production of ~12.3

440   mmolN m^{-2} d^{-1} in station B and ~1.8 mmolN m^{-2} d^{-1} in station A. The contribution of

441   vertical nutrient fluxes to primary production could thus be ~11% and ~26% in stations B

442   and A, respectively, which are comparable with the f-ratio of 0.14-0.20 previously

443   estimated in the nSCS from late March to October (Chen, 2005). In steady status, the net

444   primary production of phytoplankton should be balanced by the upward nutrient flux as

445   well as the downward particle flux. Therefore, a high nutrient flux would correspond to a

446   high net primary production and thus a high biomass accumulation, if other conditions

447   remain the same (species, temperature, light, grazing, etc). Station C_9 is interesting in that

448   the vertical nutrient fluxes are net downward out of euphotic zone, suggesting that the

449   station may not be in steady status. High nutrients here are likely a result of strong

450   horizontal input or a previous diapycnal nutrient injection. In this case, large drawdown

451   of nutrients will be expected by fast growing phytoplankton and by the downward

452   transport of nutrients out of euphotic zone.

453   Uncertainty of the vertical nutrient flux could be contributed by errors in the

454   determinations of vertical diffusivity and vertical velocity, as well as nutrient

455   concentration and gradient. Calculation errors of vertical diffusivity by the Thorpe-scale

456   approach, estimated from the time-series station S_1, were 0.87 ×10^{-4} m^{-2} s^{-1} at 50 m (n=5),

457   0.71 ×10^{-4} m^{-2} s^{-1} at 100 m (n=6), and 0.46 ×10^{-4} m^{-2} s^{-1} at 150 m (n=7). We therefore

458   obtain an average of 0.68 ×10^{-4} m^{-2} s^{-1} for the overall uncertainty of diffusivity

459   determined in our study. Uncertainty of vertical velocity by Ekman pumping from

460   satellite observations could be approximately determined at each station by their standard

461   deviations over the sampling duration of May 14th-16th, 2014. Measurement errors of

462   nutrients at depths during the field study should be negligible as the concentrations are

463   considerably higher than the detection limits of the analytical methods. We are not able to

464 quantify the uncertainty of nutrient gradient, as we have only one cast for each station

465 with reduced resolution below the euphotic layer. Meanwhile, the nutrient gradient and

466 related diffusive flux that we have calculated at the base of euphotic zone could be

467 interpreted as a mean value between the two adjacent bottle depths (100-200 m). The

468 final uncertainties for the vertical nutrient fluxes are summarized in Table 1, which vary

469 substantially from 0.10 to 0.98 mmol m^{-2} d^{-1} (n=10) for stations in the offshore regions.

470

471 4.2 Impact of growth-grazing dynamics on phytoplankton chlorophyll biomass in the

472 nSCS

473   Distributions of phytoplankton in the ocean are controlled by complex physical and

474 biological interactions. To assess the influence of growth-grazing dynamics on

475 phytoplankton chlorophyll-*a* biomass in the nSCS, two stations with distinct

476 biogeochemical settings and nutrient fluxes were selected for measurements of

477 phytoplankton growth and microzooplankton grazing rates. In addition, the community

478 response to nutrient enrichments at the two stations was assessed by continuous

479 incubations for up to four days. Previous studies indicates that surface phytoplankton

480 community in the southeast Dongsha Islands is dominated by both diatom and

481 picoplankton such as *Prochlorococcus*, while picoplankton with negligible diatoms are

482 found in the non-upwelling area south of the Taiwan Strait during late spring and early

483 summer (Yang 2009; Huang et al., 2011). Our results of substantially high phytoplankton

484 growth rates observed at station B southeast of Dongsha Islands are in agreement with its

485 high nutrient concentrations and nutrient fluxes compared to station A south of Taiwan

486 Strait. When released from the constraints by nutrient limitation, phytoplankton

487 community will be expected to shift from dominance by picoplankton toward a higher

488 relative abundance of larger phytoplankton because of their higher intrinsic capacity for

489 growth (Agawin et al., 2000).

490   Percentage of the primary production consumed by microzooplankton can be

491 estimated by the ratio of microzooplankton grazing over phytoplankton growth (g/μ)

492 (Landry et al., 1998). High g/μ ratios (~1.5) at station A suggest an elevated role of the

493 microbial food web in the south Taiwan Strait, promoting nutrient recycling to support

494 further phytoplankton growth. Whereas, the relatively higher microzooplankton grazing

495   rate but lower g/μ ratio at station B may indicate a greater efficiency of carbon export

496   near the Dongsha Islands, as the greater loss of diatoms through sinking or grazing by

497   mesozooplankton in regions with high nutrient supply (Landry et al., 1998). Natural

498   growth of phytoplankton at station B was much higher than its grazing mortality, leading

499   to a large net growth rate (growth minus grazing) of 0.58 d^{-1}, which is consistent with the

500   high integrated chlorophyll biomass in this station. In contrast, a negative net growth rate

501   of -0.15 d^{-1} was found at station A as a result of higher grazing pressure. The specific

502   phosphate consumption rate of 1.03 d^{-1} at station A was about twice of that at station B

503   (0.46 d^{-1}) suggesting a larger nutrient demand at station A. There was actually a faster

504   response of phytoplankton to nutrient enrichment at station A than at station B indicating

505   a stronger nutrient limitation in the south Taiwan Strait. The negative net community

506   growth and the higher nutrient consumption rate at station A are consistent with the

507   spring phytoplankton bloom of the southwest Taiwan observed in the satellite data (Fig.

508   2c) being in its decline phase. Indeed, the area of the phytoplankton bloom decreased

509   substantially within two weeks and was not visible by the middle of June, 2014 (from

510   weekly mean sea surface chlorophyll-*a* data of MODIS Aqua) supporting the important

511   role of grazing activity on phytoplankton distribution in the nSCS.

512   In conclusion, we have conducted a preliminary study on vertical nutrient fluxes and

513   phytoplankton dynamics in the nSCS. Our results suggest that phytoplankton patchiness

514   in the nSCS during the spring inter-monsoon of May 2014 was largely controlled by

515   vertical nutrient fluxes, which were driven by both turbulent diffusion and wind stress

516   curl-driven upwelling. Our results also revealed an increasing role of turbulent diffusion

517   but a decreasing role of curl-driven upwelling on vertical transport of nutrients from the

518   coastal ocean zones to the offshore pelagic zones in the nSCS. Elevated nutrient fluxes

519   observed near the Dongsha Islands were found to support high new production leading to

520   net growth of phytoplankton community, whereas the low nutrient fluxes of the south

521   Taiwan Strait resulted in a negative net community growth leading to decline of a

522   phytoplankton bloom. As the findings presented here is limited by the very narrow area

523   and the very short period of sampling time, future studies may be improved by addressing

524   the variability of vertical nutrient fluxes and its relationship to phytoplankton dynamics

525   on a much longer time scale over a much broader area of the nSCS.

533   *References*

534   Abraham, E.R.: The generation of plankton patchiness by turbulent stirring, Nature, 391,

535   577-580, 1998.

536   Agawin, N.S.R., Duarte, C.M., and Agusti, S.: Nutrient and temperature control of the

537   contribution of picoplankton to phytoplankton biomass and production, Limnol. Oceanogr., 45,

538   591-600, 2000.

539   Bombar, D., Dippner, J.W., Doan, H.N., Ngoc, L.N., Liskow, I., Loick-Wilde, N., and Voss,

540   M.: Sources of new nitrogen in the Vietnamese upwelling region of the South China Sea, J.

541   Geophys. Res., 115, C06018, doi:10.1029/2008JC005154, 2010.

542   Centurioni, L.R., Niiler, P.P., and Lee, D.K.: Observations of inflow of Philippine Sea surface

543   water into the South China Sea through the Luzon Strait, J. Phys. Oceanogr., 34, 113-121, 2004.

544   Chao, S.Y., Shaw, P.T., and Wu, S.Y.: Deep water ventilation in the South China Sea,

545   Deep-Sea Res., I 43, 445-466, 1996.

546   Chen, B., Liu, H., Landry, M.R., Dai, M., Huang, B., and Sun, J.: Close coupling between

547   phytoplankton growth and microzooplankton grazing in the western South China Sea, Limnol.

548   Oceanogr., 54, 1084-1097, 2009.

549   Chen, B., Zheng, L., Huang, B., Song, S., and Liu, H.: Seasonal and spatial comparisons of

550   phytoplankton growth and mortality rates due to microzooplankton grazing in the northern South

551   China Sea, Biogeosciences, 10, 2775-2785, 2013.

552   Chen, Y.L.: Spatial and seasonal variations of nitrate-based new production and primary

553   production in the South China Sea, Deep-Sea Res., II, 52, 319-340, 2005

554   Chow, C., Hu, J., Centurioni, L.R., and Niiler, P.P.: Mesoscale Dongsha cyclonic eddy in the

555   northern South China Sea by drifter and satellite observations, J. Geophys. Res., 113, C04018,

556   doi:10.1029/2007JC004542, 2008.

557   Cullen, J.J., Franks, P.J.S., Karl, D.M., and Longhurst, A.: Physical influences on marine

558   ecosystem dynamics, in: The sea, 12, Robinson, A.R., McCarthy, J.J., Rothschild, B.J. (eds), John

559   Wiley & Sons, New York, 297–336, 2002.

560   Davis, C.S., Flierl, G.R., Wiebe, P.H., and Franks, P.J.S.: Micropatchiness, turbulence and

561   recruitment in plankton, J. Mar. Res., 43, 109-151, 1991.

562   Eppley, R.W., and Peterson, B.J.: Particulate organic matter flux and planktonic new

563   production in the deep ocean, Nature, 282, 677-680,1979.

564   Farris, A., and Wimbush, M.: Wind-induced intrusion into the South China Sea, J. Oceanogr.,

565   52, 771–784, 1996.

566   Galbraith, P.S., and Kelley, D.E.: Identifying Overturns in CTD Profiles, J. Atmos. Ocean.

567   Tech., 13, 688–702, 1996.

568   Gan, J., Lu, Z., Dai, M., Cheung, A., Liu, H., and Harrison, P.: Biological response to

569   intensified upwelling and to a river plume in the northeastern South China Sea: A modeling study,

570   J. Geophys. Res., 115, doi: 10.1029/2009jc005569, 2010.

571   Gargett, A. E., and Garner, T.: Determining Thorpe scales from ship-lowered CTD density

572   profiles, J. Atmos. Ocean. Tech., 25, 1657–1670, 2008.

573   Gaube, P., Chelton, D.B., Strutton, P.G., and Behrenfeld, M.J.: Satellite observations of

574   chlorophyll, phytoplankton biomass, and Ekman pumping in nonlinear mesoscale eddies, J.

575   Geophys. Res., 118, 6349-6370, doi:10.1002/2013JC009027, 2013.

576   Gill, A.E. (Eds.): Atmosphere-Ocean Dynamics, International Geophysics Series, 30,

577   Academic Press, London, 1982.

578   Han, A., Dai, M., Gan, J., Kao, S., Zhao, X., Jan, S., Li, Q., Lin, H., Chen, C., Wang, L., Hu,

579   J. Wang, L., and Gong. F.: Inter-shelf nutrient transport from the East China Sea as a major

580   nutrient source supporting winter primary production on the northeaster South China Sea shelf,

581   Biogeosciences, 10, 8159-8170, 2013.

582   Huang, B., Xiang, W., Zeng, X., Chiang, K., Tian, H., Hu, J., Lan, W., and Hong. H.:

583   Phytoplankton growth and microzooplankton grazing in a subtropical coastal upwelling system in

584   the Taiwan Strait, Cont. Shelf Res, 31, 48-56, 2011.

585   Kim, T.K., Lee, K., Duce, R., Liss, P.: Impact of atmospheric nitrogen deposition on

586   phytoplankton productivity in the South China Sea, Geophys. Res. Letters, 41(9), 3156-3162,

587   2013.

588   Klein, P., and Lapeyre, G.: The oceanic vertical pump induced by mesoscale and

589   submesoscale turbulence, Annu. Rev. Mar. Sci., 1, 351-375, 2009.

590   Landry, M.R., Brown, S.L., Campbell, L., Constantinou, J., and Liu, B.: Spatial patterns in

591   phytoplankton growth and microzooplankton grazing in the Arabian Sea during monsoon forcing,

592   Deep-Sea Res., II, 45, 2353-2368, 1998.

593   Landry, M.R., and Hassett, R. P.: Estimating the grazing impact of marine micro-zooplankton,

594   Mar. Biol., 67(3), 283-288, 1982.

595   Li, Q.P., Franks, P.J.S., and Landry, M.R.: Microzooplankton grazing dynamics:

596   parameterizing grazing models with dilution experiment data in the California Current Ecosystem,

597   Mar. Ecol. Prog. Ser., 438, 59-69, 2011.

598   Li, Q.P., Franks, P.J.S., Ohman, M.D., and Landry, M.R.: Enhanced nitrate flux and biological

599   processes in a frontal zone of the California Current System, J. Plankton Res., 34, 790-801, 2012.

600   Li, Q.P., and Hansell, D.A.: Nutrient distribution in baroclinic eddies of the oligotrophic

601 North Atlantic and inferred impacts on biology, Deep-Sea Res., II, 55, 1291-1299, 2008.

602 Li, Q.P., Hansell, D.A., and Zhang, J.Z.: Underway monitoring of nanomolar nitrate plus

603 nitrite and phosphate in oligotrophic seawater, Limnol. Oceanogr. Methods, 6, 319-326, 2008.

604 Li, Q.P., Wang, Y., Dong, Y., and Gan, J.: Modeling long-term change of planktonic

605 ecosystems in the Northern South China Sea and the upstream Kuroshio Current, J. Geophys.

606 Res., 120, doi:10.1002/2014JC010609, 2015

607 Lien, R., Tang, T., Chang, M., and D'Asaro, E.A.: Energy of nonlinear internal waves in the

608 South China Sea, Geophys. Res. Lett., 32, L05615, doi:10.1029/2004GL022012, 2005.

609 Lin, I., Lien, C., Wu, C., Wong, G.T.F., Huang, C., and Chiang, T.: Enhanced primary

610 production in the oligotrophic South China Sea by eddy injection in spring, Geophys. Res. Letters,

611 37, L16602, doi:10.1029/2010GL043872, 2010.

612 Lin, I., Wong, G.T.F., Lien, C., Chien, C., Huang, C., and Chen, J.: Aerosol impact on the

613 South China Sea biogeochemistry: an early assessment from remote sensing, Geophys. Res.

614 Letters, 36, L17605, doi:10.1029/2009GL037484, 2009.

615 Liu, K.K., Chao, S.Y., Shaw, P.T., Gong, G.C., Chen, C.C., and Tang, T.Y.: Monsoon-forced

616 chlorophyll distribution and primary production in the South China Sea: observations and a

617 numerical study, Deep-Sea Res., I, 49, 1387-1412, 2002.

618 Liu, X., Furuya, K., Shiozaki, T., Masuda, T., Kodama, T.. Sato, M.. Kaneko, H.. Nagasawa,

619 M.. and Yasuda, I.: Variability in nitrogen sources for new production in the vicinity of the shelf

620 edge of the East China Sea in summer, Cont., Shelf Res., 61-62, 23-30, 2013.

621 Liu, Z.Y., and Lozovatsky, I.: Upper pycnocline turbulence in the northern South China Sea,

622 Chin. Sci. Bull., 57(18), 2302-2306, 2012.

623 McGillicuddy, D.J., Anderson, L., Bates, N., Bibby, T., Buesseler, K., Carlson, C., Davis, C.,

624 Ewart, C., Falkowski, P., Goldthwait, S., Hansell, D.A., Jenkins, W.J., Johnson, R., Kosnyrev, V.,

625 Ledwell, J.R., Li, Q.P., Siegel, D.A., and Steinberg, D.K.: Eddy-wind interactions stimulate

626 extraordinary mid-ocean plankton blooms, Science, 316, 1021-1026, 2007.

627 Osborn, T.R.: Estimates of the local rate of vertical diffusion from dissipation measurements,

628 J. Phys. Oceanogr., 10(1), 83-89, 1980.

629 Pan, X., Wong, G.T.F., Shiah, F.K., and Ho. T.Y.: Enhancement of biological production by

630 internal waves: observations in the summertime in the northern South China Sea, J. Oceanogr., 68,

631 427-437, 2012.

632 Parsons, T.R., Maita, Y., and Lalli, C.M. (Eds.): A manual of chemical and biological methods

633 for seawater analysis, Pergamum Press, Oxford, 1984.

634 Risien, C.M., and Chelton, D.B.: A global climatology of surface wind and wind stress fields

635   from eight year QuickSCAT scatterometer data, J. Phys. Oceanogr., 38, 2379-2412, 2008.

636   Rykaczewski, R.R., and Checkley, D.M.: Influence of ocean winds on the pelagic ecosystem

637   in upwelling regions, PNAS, 105(6), 1065–1970, 2008.

638   Strom, S. L., Macri, E. L., and Olson, M. B.: Microzooplankton grazing in the coastal Gulf of

639   Alaska: Variations in top-down control of phytoplankton, Limnol. Oceanogr., 52, 1480–1494,

640   2007.

641   Tian, J., Yang, Q., and Zhao, W.: Enhanced diapycnal mixing in the South China Sea. J. Phys.

642   Oceanogr., 39, 3191-3203, 2009.

643   Thorpe, S.A.: Turbulence and mixing in a Scottish loch, Phil. Trans. Royal Soc., London A,

644   286, 125–181, 1977.

645   Wang, J., and Tang, D.: Phytoplankton patchiness during spring intermonsoon in west coast

646   of South China Sea, Deep-Sea Res, II, 101, 120-128, 2014.

647   Yang, Q., Tian, J., Zhao, W., Liang, X., and Zhou, L.: Observations of turbulence on the shelf

648   and slope of northern South China Sea, Deep-Sea Res., I, 87, 43-52, 2014.

649   Yang, Y.H.: Phytoplankton community structure of the northern South China Sea and the

650   Philippine Sea, Master Thesis (in CHN), National Taiwan Normal University, Taiwan, 73 pp.,

651   2009.

652   Zhou, L., Tan, Y., Huang, L., Huang, J., Liu, H., and Lian, X.: Phytoplankton growth and

653   microzooplankton grazing in the continental shelf area of northeastern South China Sea after

654   typhoon Fengshen, Cont. Shelf Res., 31, 1663-1671, 2011.

Table 1: Comparisons of integrated chlorophyll-a ($\int Chl \cdot dz$), nitrate gradient ($\partial C/\partial z$), nitrate concentration (NO_3), vertical diffusivity (K_z), upwelling velocity (w_e), diffusive nitrate flux (J_{dif}), upwelled nitrate flux (J_{upw}), and total nitrate flux (J_{total}) for transect stations C$_{6-12}$ and incubation stations A and B at ~1% light depth (~100m depth).

Station	$\int Chl \cdot dz$ [mg m⁻²]	$\partial C/\partial z$ [mmol m⁻⁴]	NO_3 [mmol m⁻³]	[a] K_z [10⁻⁴ m² s⁻¹]	[b] w_e [10⁻⁵ m s⁻¹]	J_{dif} [mmol m⁻² d⁻¹]	[c] J_{upw} [mmol m⁻² d⁻¹]	J_{total} [mmol m⁻² d⁻¹]
C$_6$	16.8	0.001	5.01	6.30±0.68	0.28±0.02	0.05±0.01	1.21±0.09	1.27±0.10
C$_7$	20.2	0.077	6.42	0.91±0.68	0.03±0.05	0.60±0.45	0.17±0.27	0.77±0.73
C$_8$	22.1	0.079	7.47	3.60±0.68	-0.21±0.08	2.44±0.46	-1.36±0.52	1.09±0.98
C$_9$	15.4	0.122	9.52	0.25±0.68	-0.12±0.03	0.26±0.72	-0.99±0.25	-0.72±0.96
C$_{10}$	21.7	0.082	9.37	3.45±0.68	-0.18±0.03	2.44±0.48	-1.46±0.24	0.99±0.72
C$_{11}$	38.7	0.060	2.08	3.30±0.68	-0.27±0.07	1.71±0.35	-0.49±0.13	1.23±0.48
C$_{12}$	20.7	0.029	3.93	1.53±0.68	0.05±0.05	0.39±0.17	0.17±0.17	0.56±0.34
C$_{13}$	13.2	0.046	1.98	2.26±0.68	-0.27±0.17	0.91±0.27	-0.46±0.29	0.44±0.56
A	15.7	0.047	2.09	1.60±0.68	-0.09±0.04	0.65±0.28	-0.16±0.08	0.49±0.35
B	24.8	0.080	4.82	4.40±0.68	-0.41±0.11	3.03±0.47	-1.71±0.46	1.33±0.93

[a] uncertainty of K_z from Thorpe analyses is estimated as 0.68×10^{-4} m² s⁻¹ (see text for detail)

[b] w_e are 3-day-mean of May 14th-16th, 2014, except station B that is of May 12th-14th, 2014

[c] assuming vertical velocity at the depth of 100m is equal to w_e.

663 Figure 1: Sampling map in the northeastern South China Sea during May 2014. Dash
664 lines show the topography of the study area; solid dots are the stations for a transect study
665 (C_{1-13}) during May 14th-16th, 2014; star is a time-series reference station (S_1); filled
666 squares are two stations where shipboard dilution experiments were performed (A and B).
667 Inserted plot shows the temperature/salinity diagram for the transect with arrows
668 indicating waters from the coastal ocean zone (thick gray lines), the offshore pelagic zone
669 (thick black lines), and the Kuroshio intrusion zone (thin lines).

671 Figure 2: Spatial distributions of (a) sea surface temperature, (b) curl-driven upwelling
672 velocity, and (c) sea surface chlorophyll during the survey, together with (d) the
673 time-series of curl-driven upwelling and wind stress at stations C_6 and C_{13} during
674 May-June, 2014. Vectors in panel (a) and panel (b) are surface geostrophic currents and
675 wind stresses, respectively; geostrophic current is from OSCAR data; upwelling velocity
676 and wind stress are from 3-day mean METOP-ASCAT data; sea surface temperature is
677 3-day-mean GOES-POES data; sea surface chlorophyll-*a* is monthly MODIS-Aqua data.

679 Figure 3: Vertical distributions of (a) temperature [*T*], (b) salinity [*S*], (c) chlorophyll-*a*
680 [*Chl-a*], (d) nitrate [NO_3], (e) silicate [$Si(OH)_4$], and (f) phosphate [PO_4] along the coastal
681 transect of the northern South China Sea. Overlaid white lines in each panel are
682 isopycnals.

684 Figure 4: Profiles of Thorpe displacement (d_z), Thorpe scale (L_T), and turbulent
685 diffusivity (K_z) for nine stations (C_5, C_6, C_7, C_8, C_9, C_{10}, C_{11}, C_{12}, C_{13}) from the edge of
686 continental shelf to the west of Luzon Strait. Locations of these stations are shown in
687 Figure 1.

689 Figure 5: Comparisons of vertical turbulent diffusivities (K_z) between two stations A and
690 B. Black line is the result of the reference station S_1 with continuous CTD sampling up to
691 13 casts; circles are for station A (2 casts) with squares for station B (2 casts).

693 Figure 6: Comparisons of vertical profiles of chlorophyll-*a* [*Chl-a*], temperature [*T*],
694 nutrients [$Si(OH)_4$, NO_3, PO_4], and nutrient gradients between two incubation stations A
695 and B. Thick lines in each panel are for bottom axis with thin lines (open symbols) for top
696 axis; dash lines are for station A with solid lines for station B.

698 Figure 7: Dilution experiment plots of phytoplankton net growth rates against the dilution
699 factors for stations A and B. Filled circles are net growth rates of the raw seawater
700 without nutrient enrichments.

702 Figure 8: Temporal variations of chlorophyll-*a* and phosphate during incubations with
703 and without nutrient enrichments in stations A and B. Dash lines (filled symbols) are for
704 chlorophyll-*a* in left axis with thin lines (open symbols) for phosphate in right axis;
705 control is the incubation of raw seawater without nutrient addition.
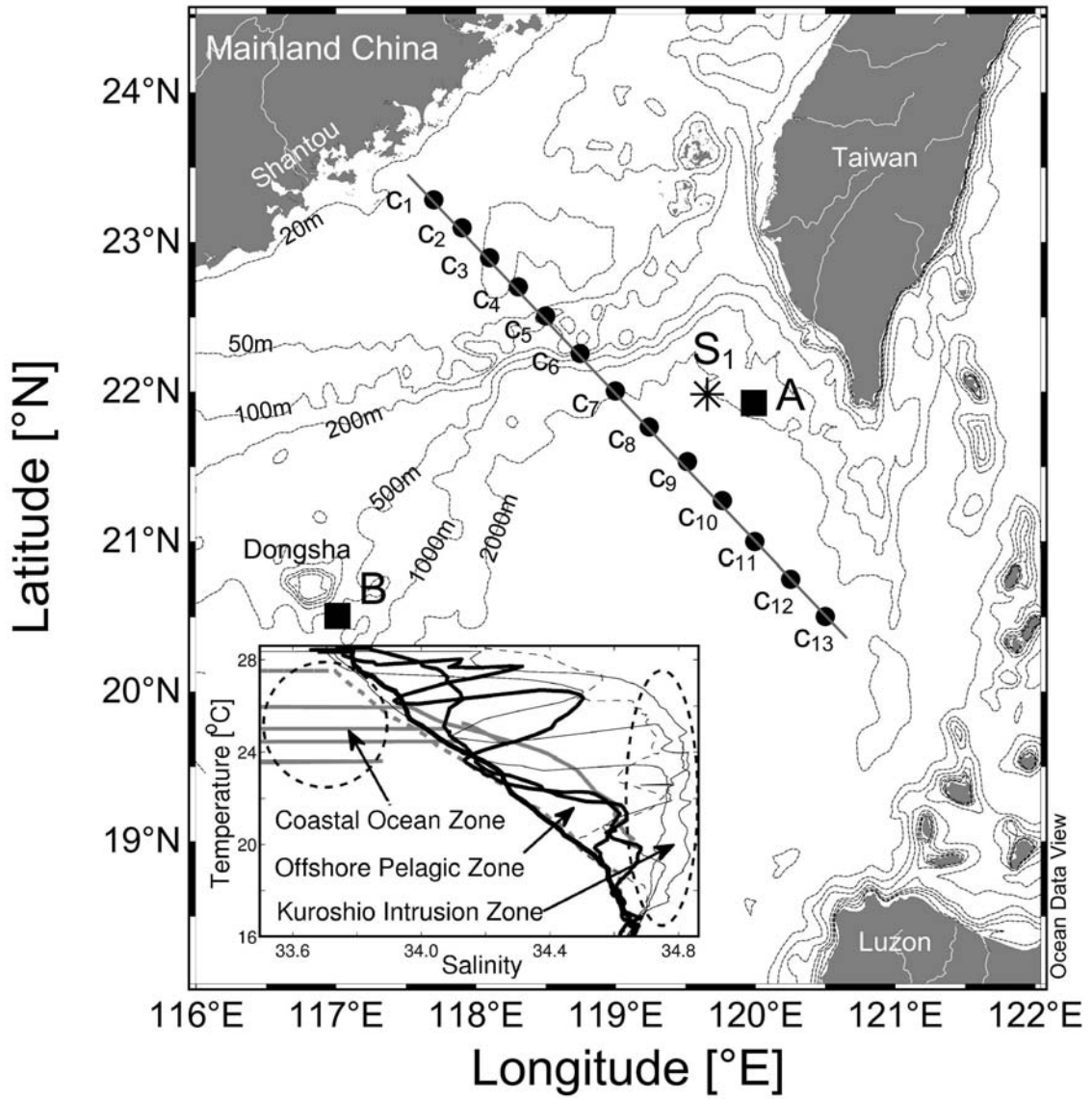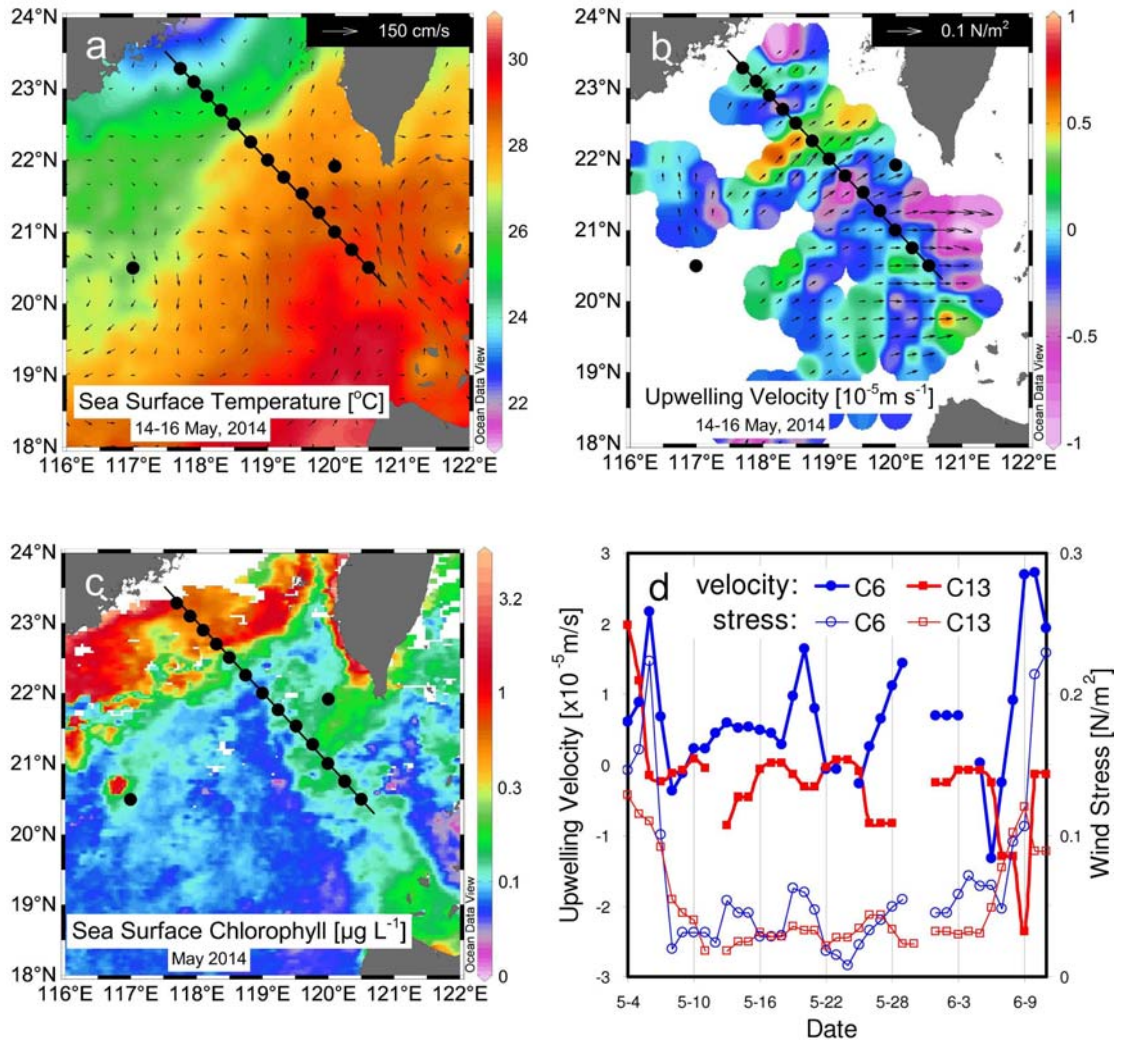
706
707
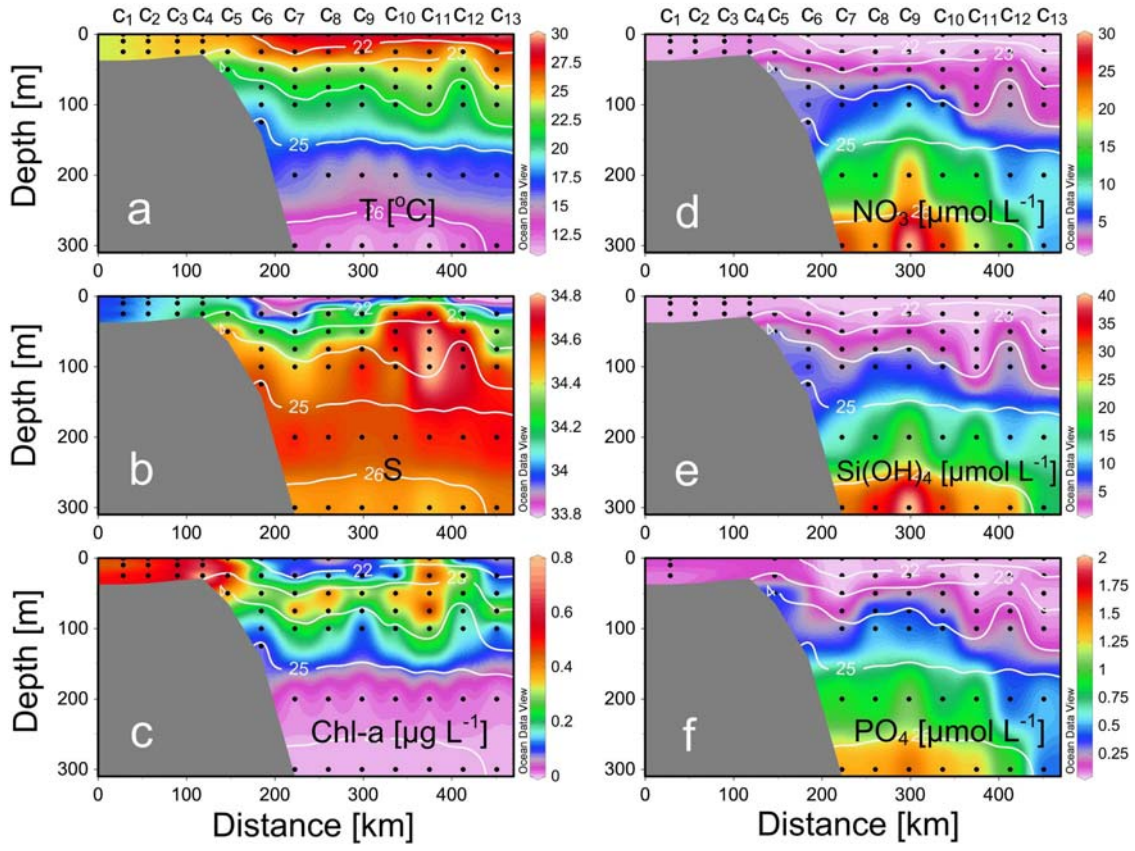708   Figure 1
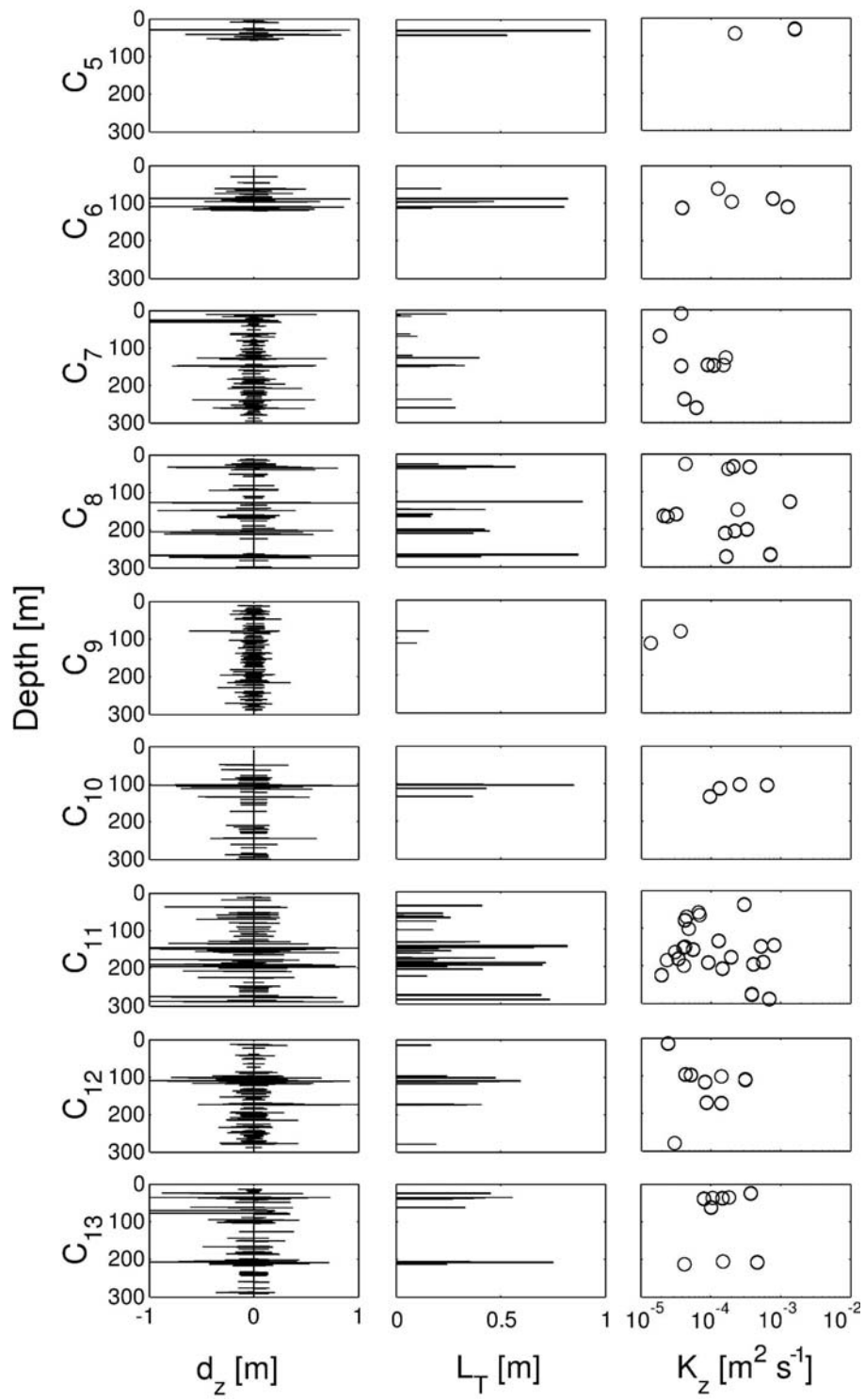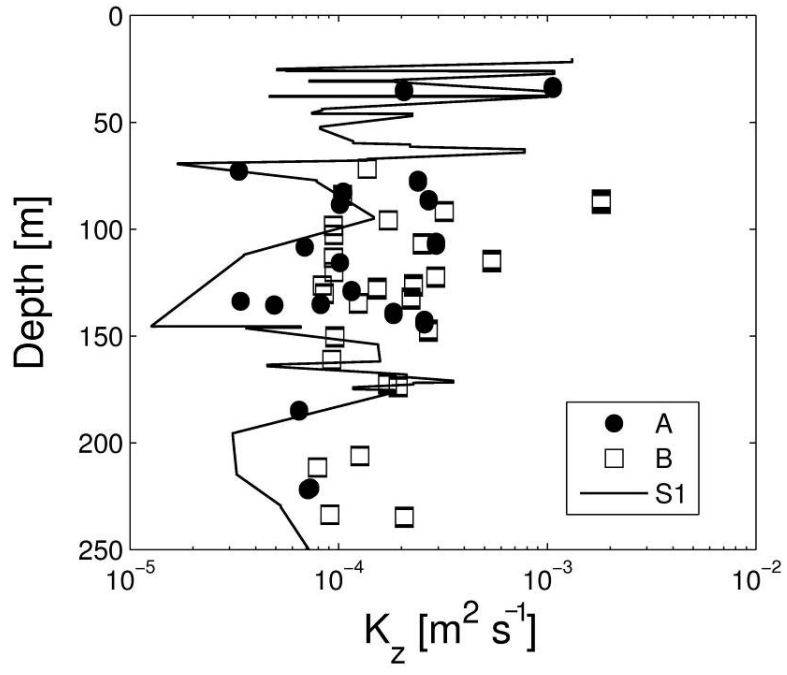
Figure 2

712

713
714 Figure 3

31

Figure 4

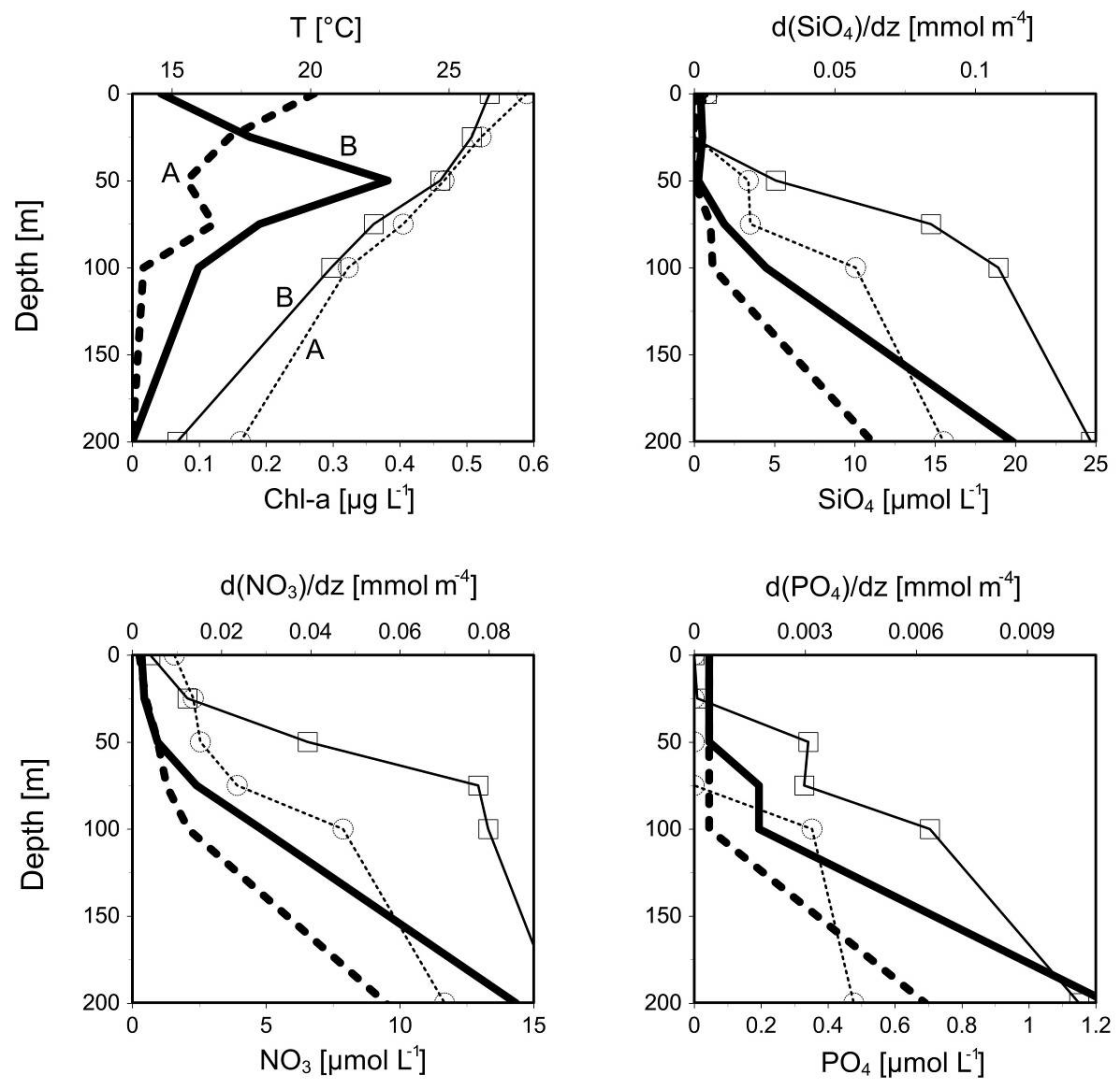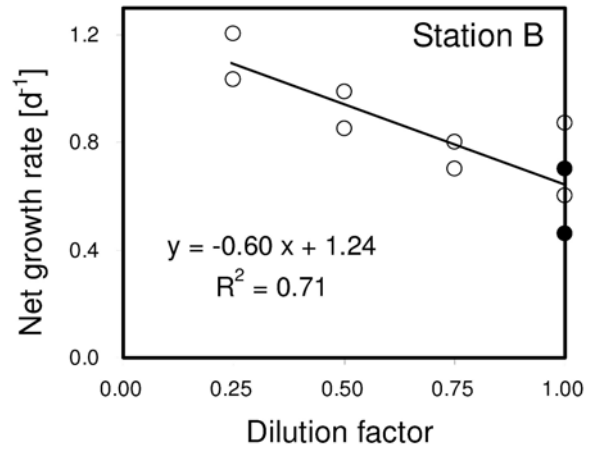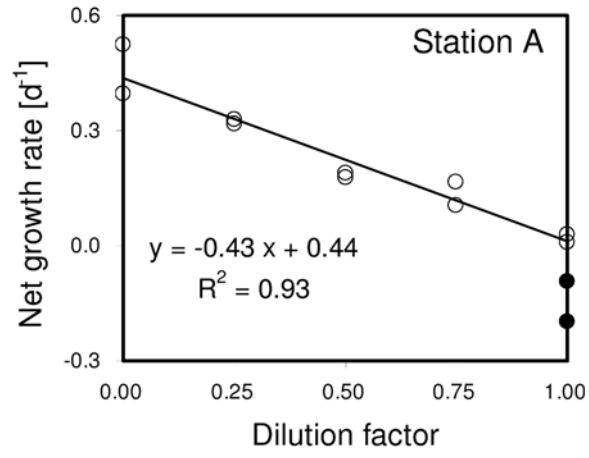Figure 5

721
722
723   Figure 6

724

725
726
727
728   Figure 7

35

729
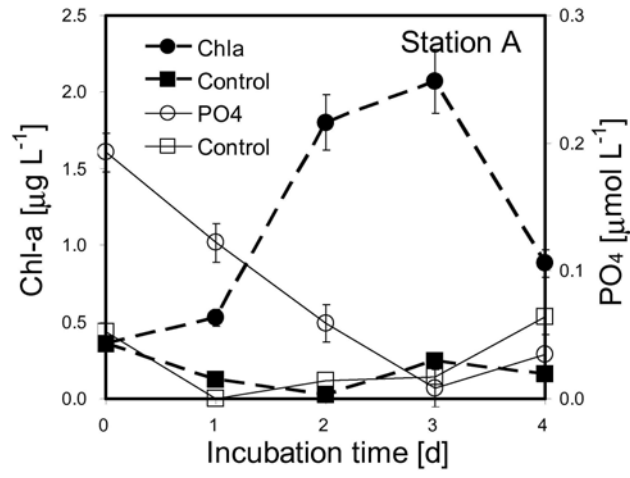

730
731
732
733   Figure 8
734
735